

Thermodynamic and shadow radius analysis of the charged Einstein-Euler-Heisenberg black hole

Yun Soo Myung*

Center for Quantum Spacetime, Sogang University, Seoul 04107, Republic of Korea

Abstract

We perform the thermodynamic and shadow radius analysis of an electrically charged black hole (EC) with electric charge q and coupling constant μ obtained from the Einstein-Euler-Heisenberg nonlinear electrodynamics. For $\mu = 0.03$, we have four solution branches of the horizon including low, hot, negative, and cold ones, while for $\mu = 0.3, 3$ there exist single branches without limitation on q . The shadow radius for the low branch is the nearly same as that for the Reissner-Norström black hole for $q < 1$ case, while one finds the $q > 1$ negative branch which is constrained by the EHT observation.

Typeset Using L^AT_EX

*e-mail address: ysmyoung@inje.ac.kr

1 Introduction

Supermassive black holes founded at the center of galaxies have played the important role in galaxy formation and galaxy evolution. The images of the M87* BH [1, 2, 3] have inspired enormous studies on the BH. The recent EHT observation has focussed on the center of our galaxy and shown promising images of the SgrA* BH [4, 5, 6]. The BH images indicated that there is a dark central region surrounded by a bright ring, which are called shadow and photon sphere (light ring) of the BH, respectively. Strong deflection lensing can generate a shadow and relativistic images caused by photons winding several loops around a BH [7, 8]. The photon sphere of a BH plays an important role in the strong deflection. Interestingly, the shadow of BH with scalar hair was employed to test the EHT results [9], while the shadows of other BHs, wormholes, and naked singularities obtained from various modified gravity theories have been used to constrain their hair parameters [10].

It is well known that the BH thermodynamics is universal and can be applicable to BHs found in various modified gravity theories. If one knows the entropy and temperature for a BH, one finds its thermal stability through the heat capacity. Also, if one has a few solution branches to the horizon, computation of their entropy and temperature makes the nature of branches clear [11, 12].

In this work, we wish to perform thermodynamic and shadow radius analysis of an electrically charged black hole (EC) with electric charge q and coupling constant μ obtained from the Einstein-Euler-Heisenberg-nonlinear electrodynamics (EEH) [13, 14, 15, 16]. Recently, there were thermodynamic studies [17, 18, 19], weak deflection angle [20], and optical appearance [21] on the black hole with electric (or magnetic) charges.

Our analysis depends critically on the coupling constant μ . For $\mu = 0.03$, we have four solution branches of the horizon including low, hot, negative, and cold ones, while for $\mu = 0.3, 3$ there exist single branches. There are naked singularity (NS) arisen from the charge extension of the light rings for the negative and cold branches. It is important to note that for $\mu = 0.3, 3$, there is no limitation on the magnetic charge q for its horizon, thermodynamic quantities, light ring, and shadow radius. Therefore, there is no NS arisen from the charge extension of the light rings for $\mu = 0.3, 3$. The shadow radii for the EC are the nearly same as that for the Reissner-Norström black hole (RN) for $q < 1$, while one finds the $q > 1$ negative branch which is constrained by the recent EHT observation. The analysis of shadow radius was discussed in the magnetically charged black hole [16, 10].

2 Electrically charged black holes

We introduce the Einstein-Euler-Heisenberg nonlinear electrodynamics (EEH) with $G = 1$ [17]

$$\mathcal{L}_{\text{EEH}} = \frac{1}{16\pi} \left[R - 4F + 2a \left(F^2 + \frac{7}{4} G^2 \right) \right], \quad F = \frac{F_{\mu\nu} F^{\mu\nu}}{4}, \quad G = \frac{{}^*F^{\mu\nu} F_{\mu\nu}}{4} \quad (1)$$

where a coupling constant $a = \frac{8\alpha^2}{45m_e^4}$ is redefined as 8μ with $\mu = \frac{\alpha^2}{45m_e^4}$ to recover the same metric function for a magnetically charged black hole (MC) [16].

To find the black hole solution, we consider a spherically symmetric spacetime and tensor $P_{\mu\nu}$ as

$$ds_{\text{EEH}}^2 = -f(r)dt^2 + \frac{dr^2}{f(r)} + r^2(d\theta^2 + \sin^2\theta d\phi^2), \quad P_{\mu\nu} = \frac{q^2}{r^2} \delta_{[\mu}^0 \delta_{\nu]}^1 \quad (2)$$

with q an electric charge. Here, the metric function takes the forms

$$f(r) = 1 - \frac{2m}{r} + \frac{q^2}{r^2} - \frac{2\mu q^4}{5r^6} \quad (3)$$

which recovers the RN in the limit of $\mu \rightarrow 0$.

From $f(r) = 0$ with $\mu = 0.03$, one finds that there are four branches (positive roots) of the horizon

$$r_L(m, q, \mu), \quad r_H(m, q, \mu), \quad r_N(m, q, \mu), \quad r_C(m, q, \mu) \quad (4)$$

whose forms are too complicated to show here. Here, $q - (q+)$ represent $q \in [0, 0.95](q \in [0.95, \infty))$. For $\mu = 0.3, 3$, there exist single branches of $r_L(m, q, \mu)$. The names of subscript are clear when its thermodynamic quantities are found: L, H, N, C imply low, hot, negative, cold, respectively. The case of $\mu = 0.03$ is similar to Einstein-Maxwell-scalar black holes with a quartic coupling function $f(\Phi) = 1 + \alpha\Phi^4$: the hot, the cold, and the bald (RN) branches [11, 12]. For a reference, we wish to include the RN solution with its event horizon and electric potential

$$r_{\text{RN}}(m, q) = m - \sqrt{m^2 - q^2}, \quad A = \frac{qdt}{r}, \quad (5)$$

which implies $0 < q/m < 1$ for existing two (event/Cauchy) horizons. From (Left) Fig. 1, one finds that $r_L(1, q, 0.3)$ and $r_L(1, q, 3)$ have single horizons without limitation of q . An important point is that there is no theoretical constraint on restricting

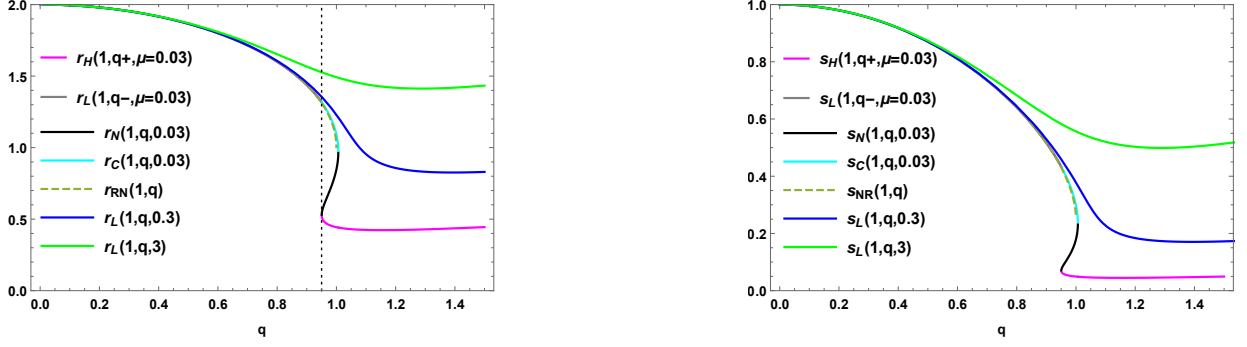


Figure 1: (Left) Four branches of the horizon $r_L(1, q-, \mu = 0.03) \geq r_C(1, q, 0.03) \geq r_N(1, q, 0.03) \geq r_H(1, q+, 0.03)$ as functions of q with $r_{RN}(1, q)$. Here, we note that $r_L(1, q, 0.3)$ and $r_L(1, q, 3)$ are defined as single horizons without limitation of q . A dotted line represents $q = 0.95$ where the low branch meets the cold one and the negative branch meets the hot one. (Right) Four reduced entropies $s_L(1, q-, \mu = 0.03) \geq s_C(1, q, 0.03) \geq s_N(1, q, 0.03) \geq s_H(1, q+, 0.03)$ as functions of q with $s_{RN}(1, q)$.

the electric charge q . On the other hand, one may have four branches for $\mu = 0.03$ which depend on the q range: $r_L(1, q-, 0.03)$, $r_C(1, q \in [0.95, 1.0065], 0.03)$, $r_N(1, q \in [1.0065, 0.95], 0.03)$, $r_H(1, q+, 0.03)$. A dotted line represents $q = 0.9503 (\simeq 0.95)$ where the low branch meets the cold one and the negative branch meets the high one. At $q = 1.0065$, the cold branch meets the negative one.

| | | | | | | |
|-------|------------|-------------|---------------|---------------|----------------|-----------|
| q | 0.5 | 0.6 | 0.7 | 0.85 | 0.9 | 0.95 |
| μ | (0,0.0002] | (0,0.001] | (0,0.002] | (0,0.011] | (0,0.018] | (0, 0.03] |
| q | 1 | 1.0065 | 1.01 | 1.015 | 1.02 | 1.021 |
| μ | (0,0.055] | [0.03,0.06] | [0.044,0.064] | [0.062,0.069] | [0.0758,0.076] | N.A. |

Table 1: μ -region for the existence of $r_N(1, q, \mu)$ and $r_C(1, q, \mu)$, depending on the electric charge q .

It is important to clarify the μ and q -regions for the existence of $r_N(m, q, \mu)$ and $r_C(m, q, \mu)$ with $m = 1$. We compute them numerically because there is no analytic result. In Table 1, we display the coupling parameter μ -region for the existence of $r_N(1, q, \mu)$ and $r_C(1, q, \mu)$, depending on the electric charge q . For $q = 0.1$, its allowed μ -range is tiny like as $(0, 1.23 \times 10^{-8}]$. As q increases from $q = 0.5$, the μ -range increases. As q increases

from $q = 1$, the μ -range becomes smaller and smaller. Its q -upper limit is $q = 1.02$ and the corresponding μ -region is small like as $[0.0758, 0.076]$ which is less than 0.1 for a given $m = 1$. This is why we choose $\mu = 0.03$ for realizing four solution branches of the horizon. It is worth noting that μ does not exist beyond $q = 1.02$. For $q \in [0.95, 1.0065]$, $\mu = 0.03$ corresponds to the upper bound as well as the lower bound, guaranteeing the existence of $r_N(1, q, \mu)$ and $r_C(1, q, \mu)$ as shown in (Left) Fig. 1. If one chooses a smaller $\mu < 0.03$, two branches of $r_N(1, q, \mu)$ and $r_C(1, q, \mu)$ exist for a smaller q -range than $q \in [0.95, 1.0065]$. This shows clearly how to develop four solution branches of the horizon according to the μ -term $(-2\mu q^4/5r^6)$ in the metric function Eq.(3).

3 Thermodynamic analysis

The mass is obtained from $f(r_i) = 0$ for $i=L, H, N, C$ as

$$M_i(m, q, \mu) = \frac{r_i(m, q, \mu)}{2} \left[1 + \frac{q^2}{r_i^2(m, q, \mu)} - \frac{2\mu q^4}{5r_i^6(m, q, \mu)} \right]. \quad (6)$$

Also, the temperature from the surface gravity and chemical (electric and μ) potentials at the horizon from $\partial M_i(m, q, \mu)/\partial q$ and $\partial M_i(m, q, \mu)/\partial \mu$ are given by

$$T_i(m, q, \mu) = \frac{\kappa}{2\pi} = \frac{f'(r_i)}{4\pi} = \frac{1}{4\pi r_i(m, q, \mu)} \left[1 - \frac{q^2}{r_i^2(m, q, \mu)} - \frac{2\mu q^4}{r_i^6(m, q, \mu)} \right], \quad (7)$$

$$W_{q,i}(m, q, \mu) = \frac{q}{r_i(m, q, \mu)} - \frac{4\mu q^3}{5r_i^5(m, q, \mu)}, \quad W_{\mu,i}(m, q, \mu) = -\frac{q^4}{5r_i^5(m, q, \mu)}. \quad (8)$$

Here, we note that $T_i(m, q, \mu)$ can be obtained from replacing S_i by πr_i^2 after considering $\partial M_i(S_i, q, \mu)/\partial S_i$. With the area-law entropy and temperature T_i , we check that the first law [19]

$$dM_i(m, q, \mu) = T_i(m, q, \mu)dS_i(m, q, \mu) + W_{q,i}(m, q, \mu)dq + W_{\mu,i}(m, q, \mu)d\mu \quad (9)$$

is satisfied. Furthermore, it is shown that the Smarr formula expressing the relation between the thermodynamic quantities is satisfied as

$$M_i(m, q, \mu) = 2T_i(m, q, \mu)S_i(m, q, \mu) + W_{q,i}(m, q, \mu)q + 2W_{\mu,i}(m, q, \mu)\mu. \quad (10)$$

In (Right) Fig. 1, we display the reduced entropy defined by $s_i(m, q, \mu) = S_i(m, q, \mu)/4\pi m^2$ which shows a similar behavior as in (Left) Fig. 1. The reduced temperature defined

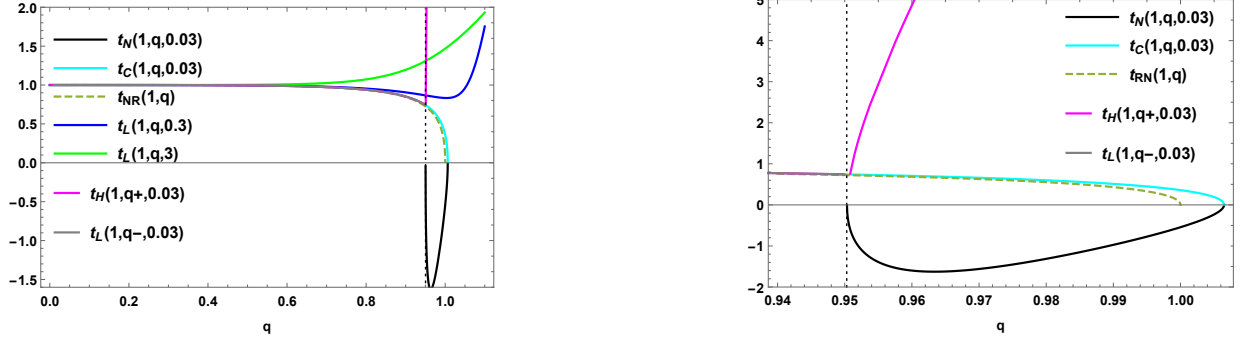


Figure 2: (Left) Several reduced temperatures $t_i(m = 1, q, \mu = 0.03)$ for $i=L, N, C, H$, $t_L(1, q, 0.3)$, $t_L(1, q, 3)$, and $t_{RN}(1, q)$ as functions of $q \in [0, 1.2]$. (Right) Enlarged reduced temperatures $t_i(1, q, 0.03)$ and $t_{RN}(1, q)$ are functions of $q \in [0.94, 1.0065]$. This shows clearly that L, H, C, N represent low, hot, cold, negative temperatures, respectively. A dotted line denotes $q = 0.95$ where five temperatures pass it.

by $t_i(m, q, \mu) = 8\pi m T_i(m, p, q)$ is shown in Fig. 2. This shows clearly why we use the subscripts L, H, C, N , representing low, high, cold, negative temperatures, respectively. A dotted line denotes $q = 0.95$ at which five temperatures pass it.

Now, we are in a position to introduce the heat capacity defined by $\partial M_i / \partial t_i$ as

$$c_i(m, q, \mu) = -\frac{r_i^2(m, q, \mu)[2\mu q^4 - q^2 r_i^4(m, q, \mu) + r_i^6(m, q, \mu)]}{4[14\mu q^4 - 3q^2 r_i^4(m, q, \mu) + r_i^6(m, q, \mu)]}. \quad (11)$$

We note that the locally thermal stability (instability) can be achieved when $c_i > 0$ ($c_i < 0$). In addition, the reduced RN temperature and heat capacity are given by

$$t_{RN}(m, q) = \frac{2}{r_{RN}(m, q)} \left[1 - \frac{q^2}{r_{RN}^2(m, q)} \right], \quad (12)$$

$$c_{RN}(m, q) = -\frac{r_{RN}^2(m, q)}{4} \frac{(r_{RN}^2(m, q) - q^2)}{(r_{RN}^2(m, q) - 3q^2)}. \quad (13)$$

From Fig. 3, one finds that three Davies lines for $c_{RN}(1, q)$, $c_L(1, q-, 0.03)$, $c_N(1, q, 0.03)$ are located at $q = 0.866, 0.871, 0.962$, $c_C \geq 0$, and $c_H(1, q+, 0.03) \leq 0$, $c_L(1, q, 0.3) \leq 0$, $c_L(1, q, 3) \leq 0$. This means that three branches including Davies points make phase transitions, the cold branch is thermodynamically stable, whereas the last three branches are always thermodynamically unstable. We have thermodynamically stable regions: $q \in [0.871, 0.95]$ for the low branch, $q \in [0.95, 1.0065]$ for the cold branch, $q \in [0.95, 0.962]$ for the negative branch, and $q \in [0.866, 1]$ for the RN branch. These regions might be related

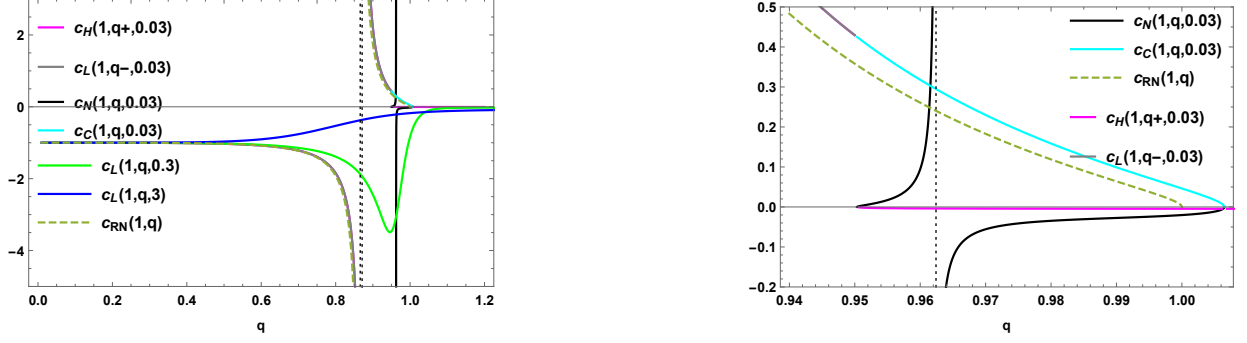


Figure 3: (Left) Several heat capacities $c_i(m = 1, q, \mu = 0.03)$ for $i=L, N, C, H$, $c_L(1, q, 0.3)$, $c_L(1, q, 3)$, and $c_{RN}(1, q)$ as functions of $q \in [0, 1.2]$. There are two Davies points (dotted lines at $q = 0.866, 0.871$). and two extremal points with $c_i = 0$. (Right) Enlarged heat capacities $c_i(1, q, 0.03)$ and $c_{RN}(1, q)$ are functions of $q \in [0.94, 1.0065]$. The dotted line indicates a Davies line at $q = 0.962$ for the negative branch and three extremal points appear as $c_i(1, q, 0.03) = 0$ with $c_{RN}(1, q) = 0$.

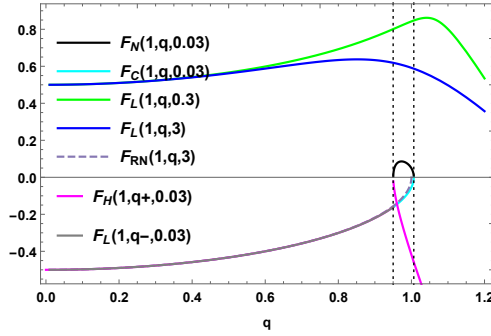


Figure 4: Several Helmholtz free energies $F_i(m = 1, q, \mu = 0.03)$ for $i=L, N, C, H$, $F_L(1, q, 0.3)$, $F_L(1, q, 3)$, and $c_{RN}(1, q)$ as functions of $q \in [0, 1.2]$. Two dotted lines indicate the zero free energy at $q = 0.95$ and 1.0065 where the latter is considered as an extremal point.

to the shadow radii predicted by the EHT observation. Finally, we need the Helmholtz free energy to test the global stability. If it is positive (negative), it is globally unstable (stable). In this case, we introduce the ground state as an extremal black hole for $\mu = 0.03$ like as the RN case. The Helmholtz free energy is defined as $F_i = M_i - T_i S_i - M_{e,i}$ with the RN

free energy

$$F_i(m, q, \mu) = \frac{r_i(m, q, \mu)}{4} + \frac{3q^2}{r_i(m, q, \mu)} - \frac{7\mu q^4}{10r_i^5(m, q, \mu)} - M_{e,i}. \quad (14)$$

$$F_{RN}(m, q) = \frac{r_{RN}(m, q)}{4} + \frac{3q^2}{r_{RN}(m, q)} - M_{e,RN}. \quad (15)$$

As is shown in Fig. 4, the Helmholtz free energy for $\mu = 0.3, 3$ are positive for $q \in [0, 1.2]$ because they do not include extremal points. This means that they are globally unstable. However, three branches of $r_L(1, q-, 0.03), r_H(1, q+, 0.03), r_C(1, q, 0.03)$ with $r_{RM}(1, q)$ are globally stable except that the negative branch is globally unstable.

4 Light rings and shadow radii

We introduce the Lagrangian of the photon to find the light rings of the EC

$$\mathcal{L}_{LR} = \frac{1}{2}g_{\mu\nu}\dot{x}^\mu\dot{x}^\nu = \frac{1}{2}\left[-f(r)\dot{t}^2 + \frac{\dot{r}^2}{f(r)} + r^2(\dot{\theta}^2 + \sin^2\theta\dot{\phi}^2)\right]. \quad (16)$$

Taking the light traveling on the equatorial plane of the EC ($\theta = \pi/2$ and $\dot{\theta} = 0$) described by a spherically symmetric and static metric Eq.(2), two conserved quantities of photon (energy and angular momentum) are given by

$$E = -\frac{\partial\mathcal{L}_{LR}}{\partial\dot{t}} = g(r)\dot{t}, \quad \tilde{\ell} = \frac{\partial\mathcal{L}_{LR}}{\partial\dot{\phi}} = r^2\dot{\phi}. \quad (17)$$

Choosing the null geodesic for the photon ($ds^2 = 0$) with the affine parameter $\tilde{\lambda} = \lambda\tilde{\ell}$ and impact parameter $\tilde{b} = \tilde{\ell}/E$, its radial equation of motion is given by

$$\frac{dr}{d\tilde{\lambda}} = \sqrt{\frac{1}{\tilde{b}^2} - \frac{f(r)}{r^2}}. \quad (18)$$

Here, the effective potential for a photon takes the form

$$V(r) = \frac{f(r)}{r^2}. \quad (19)$$

Requiring the light ring (photon sphere: $\dot{r} = 0, \ddot{r} = 0$), one finds two conditions

$$V(r = L) = \frac{1}{2\tilde{b}^2}, \quad V'(r = L) = 0, \quad (20)$$

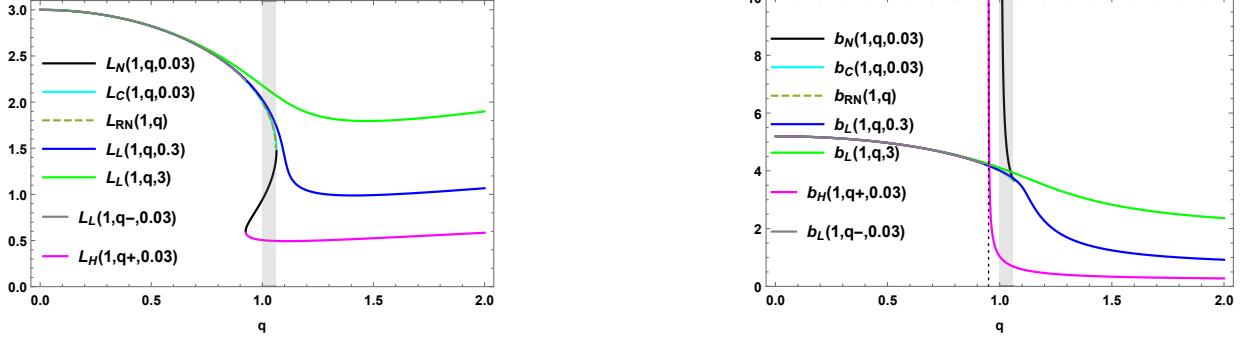


Figure 5: (Left) Four light rings $L_i(m = 1, q, \mu = 0.03)$ for $i=L, H, N, C$ and $L_L(1, q, 0.3)$, $L_L(1, q, 3)$, $L_{RN}(1, q)$ are as functions of q . The N, C, RN-branches are extended to include their NS versions defined in the shaded column ($q \in [1, 1.06]$). (Right) Four critical impact parameters $b_i(m = 1, q, \mu = 0.03)$ for $i=L, H, N, C$ and $b_L(1, q, 0.3)$, $b_L(1, q, 3)$, $b_{RN}(1, q)$ are as functions of q . A dotted line represents $q = 0.95$ which is a blow-up point for $b_H(1, q+, 0.03)$. A shaded column ($q \in [1, 1.06]$) includes their N, C, RN-NS branches.

where b denotes the critical impact parameter and L represents the radius of unstable light ring.

Eq.(20) implies two relations

$$L_i^2 = f(L_i)b_i^2, \quad 2f(L_i) - L_i f'(L_i) = 0. \quad (21)$$

Here, four light rings and their critical impact parameters ($i = L, H, N, C$) for the EC are given by

$$L_i(m, q, \mu), \quad (22)$$

$$b_i(m, q, \mu), \quad (23)$$

whose explicit forms are too complicated to write down here. For a reference, we need to have the light ring and critical impact parameter for the RN as

$$L_{RN}(m, q) = \frac{3m}{2} \left[1 + \sqrt{1 - \frac{8q^2}{9m^2}} \right], \quad b_{RN}(m, q) = \frac{3m(1 + \sqrt{1 - 8q^2/9m^2})}{\sqrt{2 + \frac{3m^2(1 + \sqrt{1 - 8q^2/9m^2})}{2q^2}}}. \quad (24)$$

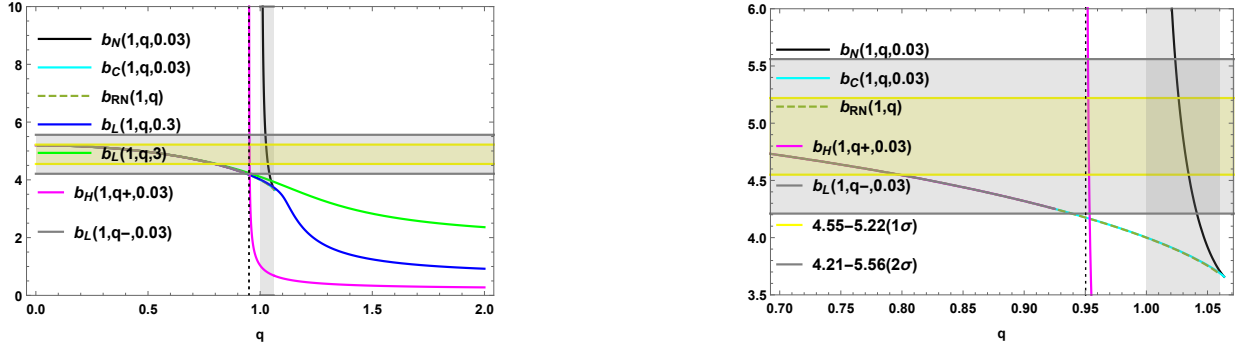


Figure 6: (Left) Several critical impact parameters $b_i(m = 1, q, \mu = 0.03)$ for $i=L, N, C, H$, $b_L(1, q, 0.3)$, $b_L(1, q, 3)$, and $b_{RN}(1, q)$ as functions of $q \in [0, 2]$. There is one blow-up (dotted line) at $q = 0.95$. Here, we introduce 1σ and 2σ ranges. (Right) Enlarged critical impact parameters $b_i(1, q, 0.03)$ and $b_{RN}(1, q)$ are functions of $q \in [0.70, 1.06]$. The dotted line at $q = 0.95$ indicates a blow-up for the hot branch. The shaded column includes the negative-NS, cold-NS, and RN-NS branches.

(Left) Fig. 5 shows the light rings and (Right) Fig. 5 represents shadow radii. We note that $L_N(1, q, 0.03)$ and $L_C(1, q, 0.03)$ are present as connectors appearing between $L_L(1, q-, 0.03)$ and $L_H(1, q+, 0.03)$, while $L_L(1, q, 0.3)$ and $L_L(1, q, 3)$ are single functions of q . From analyzing $L_{RN}(1, q)$, one finds that its q -range is extended from $[0, 1]$ to $[0, \sqrt{9/8} = 1.06]$. This implies that $q \in [1, 1.06]$ (shaded column) denotes the RN-NS branch. Also, $L_N(1, q, 0.03)$ and $L_C(1, q, 0.03)$ are extended to enter their NS branches (N-NS, C-NS) into this column. Importantly, the dotted line in (Right) Fig. 5 indicates the blow-up point for $b_H(1, q+, 0.03)$ and a shaded column ($q \in [1, 1.06]$) includes their N, C, RN-NS branches.

5 Test with EHT observation

Consulting the EHT observation (Keck- and VLTI-based estimates for SgrA* [4, 5, 6]), the 1σ constraint on the shadow radius $r_{\text{sh}} = b_i$ indicates [10]

$$4.55 \lesssim r_{\text{sh}} \lesssim 5.22 \quad (25)$$

and the 2σ constraint shows

$$4.21 \lesssim r_{\text{sh}} \lesssim 5.56. \quad (26)$$

Let us see Fig. 6 for explicit pictures for testing with the EHT observation. For the low branch of the EC, one has two constraints of the upper limits on its electric charge q : $q \lesssim 0.798(1\sigma)$ and $0.953(2\sigma)$ for $\mu = 0.03$; $q \lesssim 0.799(1\sigma)$ and $0.941(2\sigma)$ for $\mu = 0.3$; $q \lesssim 0.806(1\sigma)$ and $0.961(2\sigma)$ for $\mu = 3$. Also, one has a narrow constraint of $0.925 \lesssim q \lesssim 0.94(2\sigma)$ for the cold branch. There is no constraint for the hot branch because $b_H(1, q+, 0.03)$ is a nearly vertical line. Similarly, the RN is constrained as $q \lesssim 0.798(1\sigma)$ and $0.939(2\sigma)$. The EHT observation rules out the possibility of SgrA* being an extremal RN ($q_{eRN} = 1$) and the RN-NS branch ($q \in [1, 1.06]$: shaded column) is excluded from $q \lesssim 0.939(2\sigma)$ [10].

From (Right) Fig. 6, one observes that two narrow ranges of $1.026 \lesssim q \lesssim 1.035(1\sigma)$ and $1.024 \lesssim q \lesssim 1.041(2\sigma)$ exist for the negative-NS branch. We note that the cold-NS branch is ruled out by the 2σ . Also, it is worth noting that there is no $q > 1$ range which constrains its magnetic charge for $\mu = 0.3, 3$ because their critical impact parameters are monotonically decreasing functions of q [see (Left) Fig. 6].

6 Discussions

The shadow radii of various BH and NS found from modified gravity theories were extensively used to test the EHT results for SgrA* BH [4, 5, 6] and thus, to constrain their hair parameters [10]. The MC was employed to investigating shadow radii [16, 10].

In this work, we tested the EC for three coupling constants ($\mu = 0.03, 0.3, 3$) with the EHT observation for SgrA* by computing their shadow radii. For this purpose, we performed thermodynamic analysis on the EC. For $\mu = 0.03$, we clearly understand what four branches of the low, the negative, the hot, and the cold represent by considering their temperatures. Computing their heat capacity leads to that three branches of low, (negative), and RN including Davies points make phase transitions from negative (positive) to positive (negative) heat capacity. It is found that the hot branch is always thermodynamically stable, whereas the cold branch is always thermodynamically unstable. We showed that three branches of the low, the cold, and the hot with RN one are globally stable, while the negative branch is globally unstable by computing the Helmholtz free energy including an extremal point as the ground state. In this case, the shadow radius for the low branch is the nearly same as that for the RN for $q < 1$ case, while one finds the $q > 1$ negative-

NS branch which could be constrained by the EHT observation. A narrow constraint of $0.925 \lesssim q \lesssim 0.94(2\sigma)$ exists for the cold branch. However, there is no constraint on the hot branch because $b_H(1, q+, 0.03)$ is a nearly vertical line. The extremal point of $q = 1.0065$ is ruled out.

For $\mu = 0.3, 3$, there exist two single branches without limitation on electric charge q whose shadow radii are monotonically decreasing functions of q . This indicates no extremal points. Their heat capacities are always negative, implying that they are always thermodynamically unstable. Also, their Helmholtz free energies are positive for $q \in [0, 1.2]$, showing that they are globally unstable. Their shadow radii are very similar to that of the RN for $q < 1$, but there is no constraints for $q > 1$.

Acknowledgments

This work was supported by the National Research Foundation of Korea (NRF) grant funded by the Korea government(MSIT) (RS-2022-NR069013).

References

- [1] K. Akiyama *et al.* [Event Horizon Telescope], *Astrophys. J. Lett.* **875**, L1 (2019) doi:10.3847/2041-8213/ab0ec7 [arXiv:1906.11238 [astro-ph.GA]].
- [2] K. Akiyama *et al.* [Event Horizon Telescope], *Astrophys. J. Lett.* **875**, no.1, L4 (2019) doi:10.3847/2041-8213/ab0e85 [arXiv:1906.11241 [astro-ph.GA]].
- [3] K. Akiyama *et al.* [Event Horizon Telescope], *Astrophys. J. Lett.* **875**, no.1, L6 (2019) doi:10.3847/2041-8213/ab1141 [arXiv:1906.11243 [astro-ph.GA]].
- [4] K. Akiyama *et al.* [Event Horizon Telescope], *Astrophys. J. Lett.* **930**, no.2, L12 (2022) doi:10.3847/2041-8213/ac6674 [arXiv:2311.08680 [astro-ph.HE]].
- [5] K. Akiyama *et al.* [Event Horizon Telescope], *Astrophys. J. Lett.* **930**, no.2, L14 (2022) doi:10.3847/2041-8213/ac6429 [arXiv:2311.09479 [astro-ph.HE]].
- [6] K. Akiyama *et al.* [Event Horizon Telescope], *Astrophys. J. Lett.* **930**, no.2, L17 (2022) doi:10.3847/2041-8213/ac6756 [arXiv:2311.09484 [astro-ph.HE]].
- [7] J. M. Bardeen, W. H. Press and S. A. Teukolsky, *Astrophys. J.* **178**, 347 (1972) doi:10.1086/151796
- [8] V. Bozza, *Gen. Rel. Grav.* **42**, 2269-2300 (2010) doi:10.1007/s10714-010-0988-2 [arXiv:0911.2187 [gr-qc]].
- [9] M. Khodadi, A. Allahyari, S. Vagnozzi and D. F. Mota, *JCAP* **09**, 026 (2020) doi:10.1088/1475-7516/2020/09/026 [arXiv:2005.05992 [gr-qc]].
- [10] S. Vagnozzi, R. Roy, Y. D. Tsai, L. Visinelli, M. Afrin, A. Allahyari, P. Bambhaniya, D. Dey, S. G. Ghosh and P. S. Joshi, *et al.* *Class. Quant. Grav.* **40**, no.16, 165007 (2023) doi:10.1088/1361-6382/acd97b [arXiv:2205.07787 [gr-qc]].
- [11] J. L. Blázquez-Salcedo, C. A. R. Herdeiro, J. Kunz, A. M. Pombo and E. Radu, *Phys. Lett. B* **806**, 135493 (2020) doi:10.1016/j.physletb.2020.135493 [arXiv:2002.00963 [gr-qc]].

- [12] J. Luis Blázquez-Salcedo, C. A. R. Herdeiro, S. Kahlen, J. Kunz, A. M. Pombo and E. Radu, *Eur. Phys. J. C* **81**, no.2, 155 (2021) doi:10.1140/epjc/s10052-021-08952-w [arXiv:2008.11744 [gr-qc]].
- [13] H. Yajima and T. Tamaki, *Phys. Rev. D* **63**, 064007 (2001) doi:10.1103/PhysRevD.63.064007 [arXiv:gr-qc/0005016 [gr-qc]].
- [14] D. Amaro and A. Macías, *Phys. Rev. D* **102**, no.10, 104054 (2020) doi:10.1103/PhysRevD.102.104054
- [15] N. Bretón and L. A. López, *Phys. Rev. D* **104**, no.2, 024064 (2021) doi:10.1103/PhysRevD.104.024064 [arXiv:2105.12283 [gr-qc]].
- [16] A. Allahyari, M. Khodadi, S. Vagnozzi and D. F. Mota, *JCAP* **02**, 003 (2020) doi:10.1088/1475-7516/2020/02/003 [arXiv:1912.08231 [gr-qc]].
- [17] D. Magos and N. Bretón, *Phys. Rev. D* **102**, no.8, 084011 (2020) doi:10.1103/PhysRevD.102.084011 [arXiv:2009.05904 [gr-qc]].
- [18] Y. Zhao and H. Cheng, *Chin. Phys. C* **48**, no.12, 125106 (2024) doi:10.1088/1674-1137/ad79d4 [arXiv:2501.11075 [hep-th]].
- [19] H. Gürsel, M. Mangut and E. Sucu, [arXiv:2503.12306 [gr-qc]].
- [20] Q. M. Fu, L. Zhao and Y. X. Liu, *Phys. Rev. D* **104**, no.2, 024033 (2021) doi:10.1103/PhysRevD.104.024033 [arXiv:2101.08409 [gr-qc]].
- [21] X. X. Zeng, K. J. He, G. P. Li, E. W. Liang and S. Guo, *Eur. Phys. J. C* **82**, no.8, 764 (2022) doi:10.1140/epjc/s10052-022-10733-y [arXiv:2209.05938 [gr-qc]].